Charge-Transfer States at the Fullerene Interface Cause Nonradiative Recombination Losses in Sn-Based Perovskite Solar Cells

Peer-reviewed author version

ZARGAR, Fatemeh; DESTA, Derese; MERTENS, Sigurd; VAN LANDEGHEM, Melissa; HAMTAEI, Sarallah; PROOTH, Jeroen; Zillner, Julia; Hajhemati, Javid; SAFARI, Momo; HARDY, An; Schulz, Philip; Ahlswede, Erik; VERMANG, Bart; VANDEWAL, Koen & BOYEN, Hans-Gerd (2024) Charge-Transfer States at the Fullerene Interface Cause Nonradiative Recombination Losses in Sn-Based Perovskite Solar Cells. In: ACS Applied Energy Materials, 7 (9) , p. 3618 -3626.

DOI: https://doi.org/10.1021/acsaem.3c03086
Handle: http://hdl.handle.net/1942/45844

Charge-transfer States at the Fullerene Interface Cause Non-radiative Recombination Losses in Sn-based Perovskite Solar Cells

Fatemeh Zargar [a], Derese Desta [a], Sigurd Mertens [a], Melissa van Landeghem [a], Sarallah Hamtaei [a b c], Jeroen Prooth [a], Julia Zillner [d], Javid Hajhemati [e], Mohammadhosein Safari [a b c], An Hardy [a b c], Philip Schulz [e], Erik Ahlswede [d], Bart Vermang [a b c], Koen Vandewal [a b], Hans-Gerd Boyen[a]

[a] *Institute for Materials Research (IMO-IMOMEC), Hasselt University, Wetenschapspark 1, 3590 Diepenbeek, Belgium*

[b] *IMEC Division IMOMEC, Imec vzw Wetenschapspark 1, 3590 Diepenbeek, Belgium*

[c] *Energyville, Thor Park 8320, 3600 Genk, Belgium*

[d] Center for Solar Energy and Hydrogen Research Baden-Württemberg, Meitnerstraße 1, 70563 Stuttgart Germany

[e] *Centre national de la recherche scientique, Institut Photovoltaique d'Ile de France, 18 Boulevard Thomas Gobert, 91120 Palaiseau, France*

KEYWORDS: Sn-based perovskite solar cells, 2D/3D perovskite, PEAX additive, photovoltage loss, Fourier-transform photocurrent spectroscopy, Photoluminescent quantum yield, Electroluminescence external quantum yield

ABSTRACT: Tin-based perovskite solar cells (PSCs) are emerging as a more environmentally friendly alternative to traditional PSCs that typically contain toxic lead. Planar Sn-based perovskite solar cells were fabricated using a hydrophobic bulky molecule of phenylethylammonium ions (PEA^{+}) into the precursor solution as an additive to mitigate Sn^{4+} formation. When the fullerene derivative ICBA is used as electron transport layer the open-circuit voltage reaches 0.68 V, while the bandgap of the Sn-perovskite is 1.44 eV, giving a voltage deficit of 0.76 V. Using PCBM as electron transport layer, this deficit is 0.19 V higher. Herein, we identify through Fourier-transform photocurrent spectroscopy and luminescence measurements that interfacial charge-transfer states at the Sn-perovskite/fullerene interface are a non-radiative recombination channel. The energy of these states should be increased in order to mitigate voltage losses at the contacts.

INTRODUCTION

Organic-inorganic lead halide perovskites have inspired hopes for the scientific and industrial communities to develop new generations of printable solar cells. Lab scale devices have achieved remarkably high power conversion efficiency (PCE) beyond 25 % during recent years [1, 2]. Despite their excellent electro-optic properties, the toxicity and instability of lead perovskites restrict their application and commercialization [3, 4]. With increasing attention to environmental issues, researchers have devoted considerable efforts to explore low toxic substitute elements such as Sn^{2+}, Ge^{2+}, Bi^{3+}, and others [5, 6]. Among these alternatives, Sn-based perovskites are considered to be the best candidates for replacing lead. Firstly, they are

environmentally safer compared to lead [7] and their narrower optical band gap is within the optimum gap range as predicted by Shockley-Queisser [8]. So far, the highest PCE reported for Sn-based PSCs is approximately 14%, substantially lagging behind lead-based PSCs [9]. One of the fundamental challenges of Sn-based PSCs is the high sensitivity of Sn^{2+} to humidity to form Sn^{4+}, which has been reported to cause high level of self-p-doping and non-radiative recombination [10]. Another important challenge that contributes to the low photovoltaic performance of Sn-based PSCs is uncontrolled and rapid crystallization [11].

Among various approaches that have been suggested to overcome oxidation and non-uniform morphology of Sn-based PSCs, additive engineering is the most effective one. Adding small amounts of bulky organic cations such as butylammonium (BA) and phenylethylammonium (PEA) not only helps to improve the stability of Sn-based PSCs against oxygen due to their hydrophobic nature but also induces high-quality crystallinity and well-defined orientation, which further suppresses oxidation of Tin and reduces the number of Tin vacancies [12-18]. However, the device performance of Sn-based PSCs still lags behind that of Pb-based PSCs, mainly due to a large open circuit-voltage (V_{oc}) deficit, i.e. a large difference between eV_{oc} and the bandgap. An effective approach to address the issue of low V_{oc} involves selecting appropriate charge transport layers (CTL) with proper alignment of energy levels. One potential solution is to replace mono-adduct [6, 6]-phenyl C_{61} Butyric acid methyl ester (PCBM) with indence-C_{60} bisadduct (ICBA) which possess a higher LUMO [19, 20]. Although the positive effect of ICBA on Sn-based PSCs performance has been shown by several researchers, [9, 19, 21, 22] there is little known about the interface of the perovskite films with the CTLs.

To bridge this gap, we studied non-radiative recombination and associated voltage losses in Sn-based PSCs, with a particular focus on the nature of the perovskite/fullerene interface. We

regulate the film quality of the Sn-based perovskite film by introducing a small amount of PEABr to replace PEAI in the Tin perovskite precursor. Through a series of characterizations, the introduction of Br^- has been shown to effectively passivate defects in the Sn-based perovskite film and reduce the non-radiative recombination. Secondly, we replaced PCBM with ICBA as an ETL, which leads to a substantial increase of the device voltage, reaching 0.68 V. The origin of non-radiative recombination is investigated using a combination of Fourier transform photo spectroscopy and luminescence measurements. These measurements provide evidence for the charge-transfer (CT) states at the Sn-perovskite/fullerene interface. In the case of PCBM, these CT states result in weak sub-gap absorption and increased non-radiative recombination as compared to the ICBA case.

RESULTS AND DISCUSSION

Optoelectronic properties

To gain insights into the influence of different additives and ETLs on the photovoltaic performance, Sn-based perovskite devices were fabricated in an inverted planar architecture, Figure 1a shows the molecular structure of PCBM and ICBA as ETLs and the device stack ITO/PEDOT:PSS/Sn-perovskite/ICBA(PCBM)/BCP/Ag. The preparation of perovskite films involves a one-step process using the anti-solvent method [23]. Detailed fabrication information can be found in the experimental session of the supporting information.

Figure 1b shows the current density-voltage (*J-V*) curves of the champion solar cells under AM 1.5G illumination (100 mW/cm^2), and the corresponding photovoltaic (PV) characteristics are summarized in Table 1. The pristine $FASnI_3$ film based on PCBM exhibits a lower efficiency of 3.49%, with a V_{oc} of 0.38 V, and fill factor (FF) of 50%. The incorporation of PEAI into the precursor solution significantly improves the efficiency of PCBM-based solar cells up to

4.96%. By replacing PEAI with PEABr, the short circuit current J_{sc} is further enhanced from 15.41 mA/cm^2 to 17 mA/cm^2, resulting in a PCE of 5.18%.

However, PCBM-based devices still suffer from a low V_{oc}. Consequently, ICBA was used as an alternative ETL, resulting in a significantly higher V_{oc} of 0.68 V with a J_{sc} of 20.54 mA/cm^2, FF of 64%, and a PCE of 9.1%. Multiple devices were fabricated, and the statistics of the PV performance were presented in Figure 1c-f, confirming the reproducibility of the devices. The device with 15% PEABr as an additive and ICBA as an ETL performs the best. This data shows that besides the use of additives, the Sn-perovskite/ETL interface significantly affects V_{oc}. In the rest of paper, more insights are presented about the morphology and energetic structure of the……...

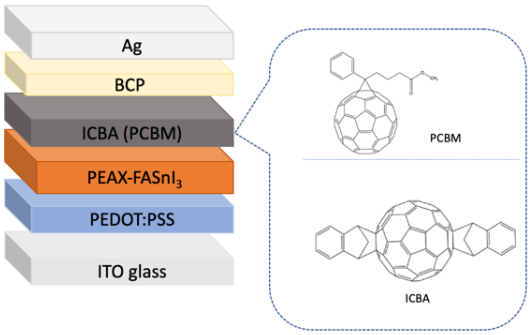

(a)

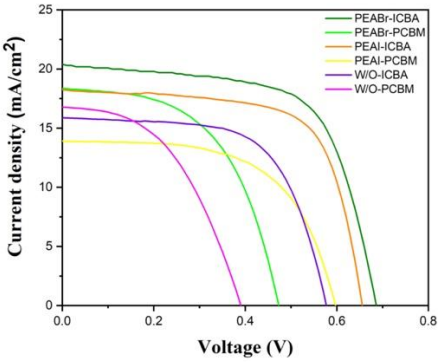

(b)

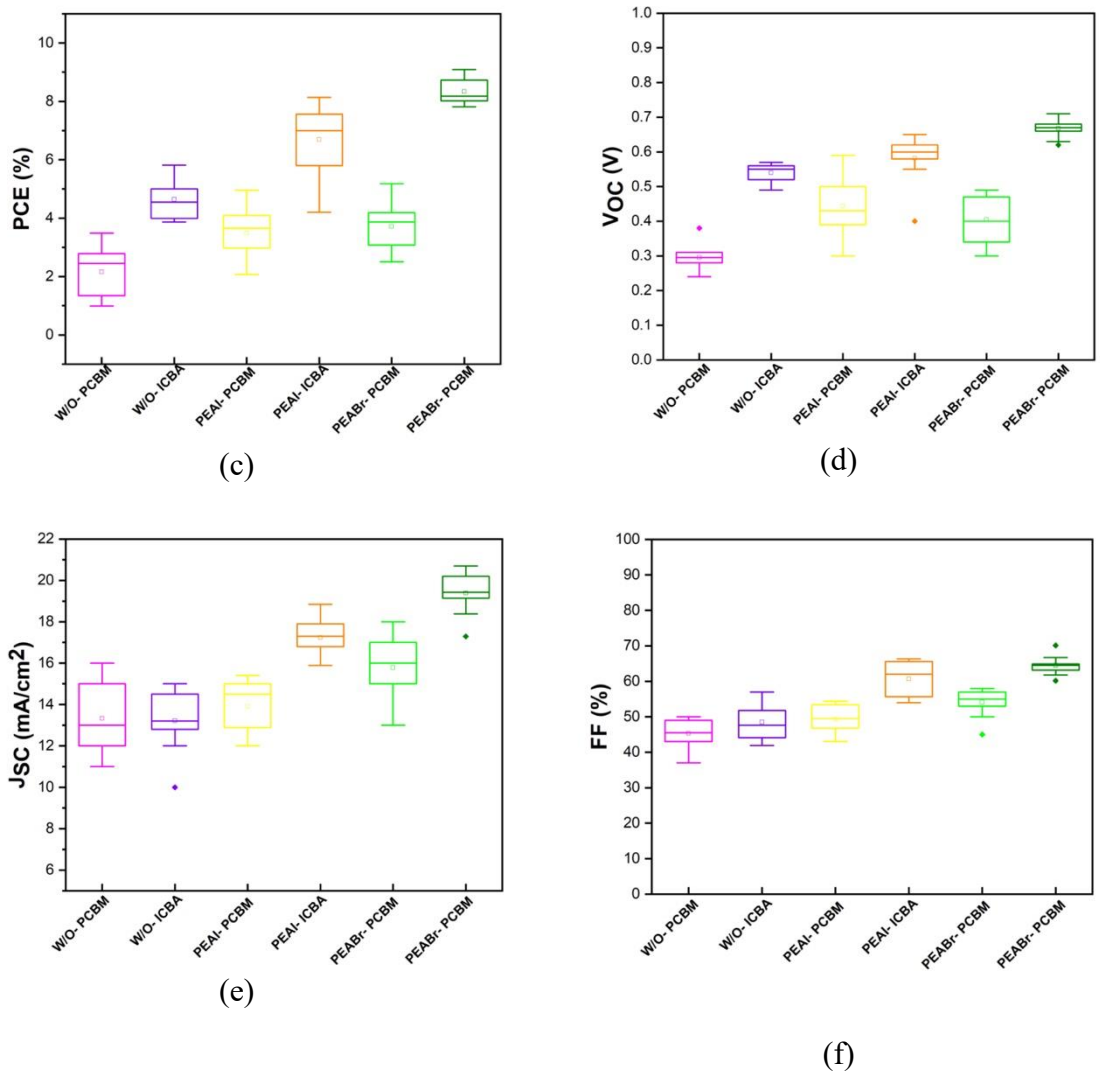

Figure 1. (a) Schematic diagram of device configuration of Sn-based PSCs. (b) Current density-voltage curves of champion solar cells of pristine $FASnI_3$ and PEAX-modified PSCs with different ETLs. Statical distribution of (c) PCE, (d) V_{oc}, (e) J_{sc}, and (f) FF of Sn-based PSCs.

Table 1. photovoltaic parameters of Sn-based PSCs.

Additive	ETL	PCE / %	V_{oc}/ V	FF / %	J_{sc}/ mAcm^{-2}
W/O	PCBM	3.49	0.38	50	18
	ICBA	5.82	0.57	57	15

PEAI	PCBM	4.96	0.59	54.37	15.41
	ICBA	8.14	0.65	66.33	18.84
PEABr	PCBM	5.18	0.49	58	17
	ICBA	9.09	0.68	64.88	20.54

Morphological and optical properties of Sn-based perovskite

Th effects of PEAX with different halides on the crystallization of the perovskite were investigated by X-ray diffraction (XRD). Figure 2a compares XRD patterns of 3D $FASnI_3$, 2D/3D PEAI-$FASnI_3$, and PEABr-$FASnI_3$ films on glass substrates. The pristine $FASnI_3$ perovskite film exhibits three main characteristic peaks assigned to the crystal planes of (100), (200), and (300), with an orthorhombic crystal structure and random orientations. Figure 2a shows that in the presence of the PEABr additive, there is a sharp increase in the peak intensity, pointing out to an increased crystallinity. This has been attributed to the fact that the radius of Br^-, introduced by the PEABr additive, is smaller than I^- [24-26].

Figure 1b-d show scanning electron microscope (SEM) images of PEAX-modified $FASnI_3$ perovskite films for different halogens. The morphology changed significantly with the addition of PEAX. The average size of crystals for 3D $FASnI_3$, 2D/3D PEAI-$FASnI_3$, and 2D/3D PEABr-$FASnI_3$ is 250 nm, 300 nm, and 350 nm, respectively. In the absence of additives, some pinholes can be seen, which leads to a rough and uneven surface and consequently a low fill factor (FF). The presence of additives enlarged the grain sizes and made the film more compact with fewer pinholes.

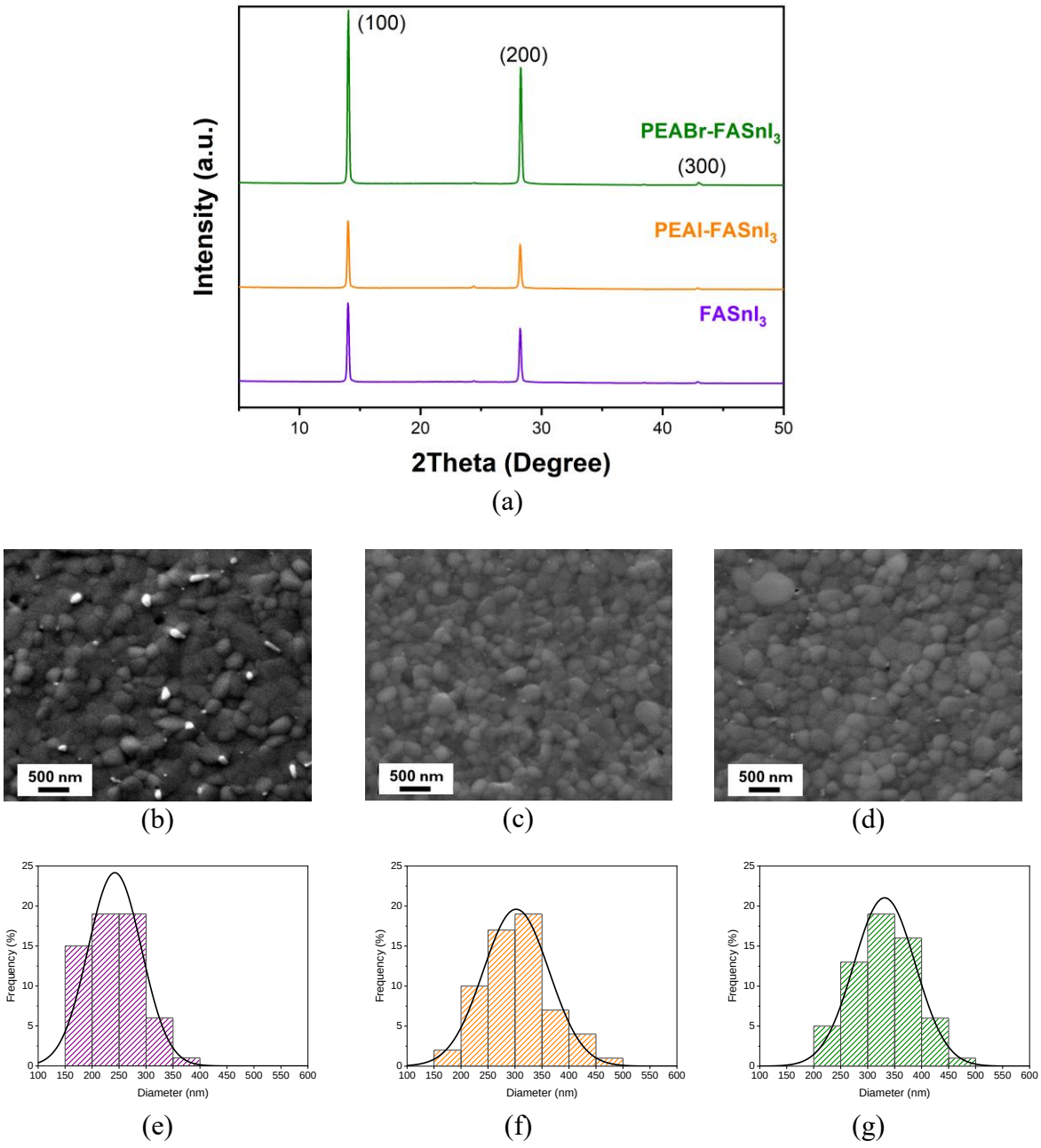

Figure 2. a) X-ray diffraction patterns, b-d) SEM images, e-g) Size distribution of 3D $FASnI_3$, 2D/3D PEAI- $FASnI_3$, and 2D/3D PEABr- $FASnI_3$ films.

The beneficial impacts of the PEABr additive on the film quality are summarized in Figure 3. The UV-vis absorption onset of PEABr-modified perovskite film shifts from 900 nm to 860 nm when I^- is replaced with Br^-, indicating an increase in the band gap from 1.37 eV to 1.44

eV (Figure 3a). This has been attributed to a slight lattice shrinkage due to the replacement of I^- by Br^-. [27] The PL spectra of PEAI-$FASnI_3$ and PEABr-$FASnI_3$ (Figure 3b) exhibit the same blue shift, which is consistent with the UV-vis results.

X-ray photoelectron spectroscopy (XPS) confirms the role of the PEABr additive in Sn^{2+} passivation during the film fabrication. Figure 3c compares the ratio of Sn^{2+} to Sn^{4+} in Sn-perovskite films with and without additive. The two deconvoluted peaks at 486.5 eV and 487.5 eV, attributed to $3d_{5/2}$ Sn^{2+} and Sn^{4+}, respectively, show that the amount of Sn^{4+} significantly decreases in the presence of PEABr additive.

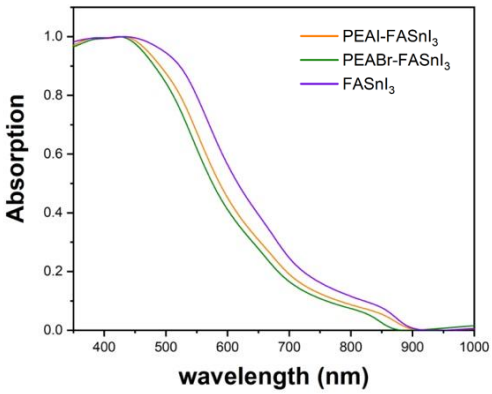

(a)

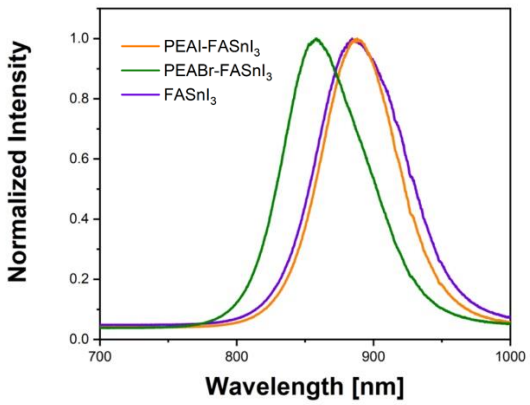

(b)

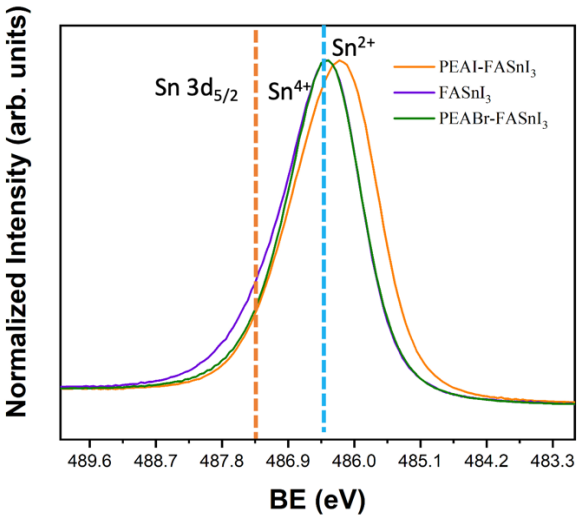

(c)

Figure 3. a) UV-vis spectra, b) steady-state PL, and c) XPS spectra of the 3d of 3D $FASnI_3$, and 2D/3D PEAX- $FASnI_3$ films.

PLQY and TR-PL of Sn-based perovskite

We now investigate the V_{oc} limitation of our PEABr-$FASnI_3$ device in more detail. To quantify the effect of the ICBA ETL on the overall non-radiative recombination and voltage losses, we carried out photoluminescence quantum yield (PLQY) and time-resolved photoluminescence (TR-PL) measurements. To exclude the influence of the atmosphere during PL measurements, all samples were encapsulated with a cover glass to ensure the reliability of the measurement. The PLQY values of different samples measured with excitation from either the film or glass side exhibited a similar trend (see supporting information). We performed PLQY measurements on both glass/Sn-perovskite and ITO/PEDOT:PSS/Sn-perovskite substrates to assess recombination in the bulk material or at the PEDOT:PSS/Sn-perovskite interface. Partial device stacks ITO/PEDOT:PSS/Sn-perovskite/ICBA (or PCBM)/BCP were used to compare the degree of interfacial recombination at ETL/Sn-perovskite interface. As can be seen in Figure 4a, the perovskite coated on the glass showed a rather high PLQY of 3.1%. However,

when the Sn-perovskite is deposited on PEDOT:PSS, the PLQY is substantially reduced from 3.1% to 0.85%. With the addition of the fullerene/BCP ETL, the PLQY reduced further to 0.51% for PCBM/BCP and 0.76% for ICBA/BCP. This indicates that, as compared to the Sn-perovskite/PCBM interface, the Sn-perovksite/ICBA interface has suppressed non-radiative recombination. However, this PLQY does not reach that of the neat film or that of the ITO/PEDOT:PSS/Sn-perovskite sample, suggesting that a significant amount of non-radiative recombination still exists at the Sn-perovskite/ICBA interface. This is confirmed by time-resolved photoluminescence (TR-PL) measurement on Sn-perovskite film with different additives on top of glass and semi-full stacks for PEABr-$FASnI_3$ with different ETLs. We extract 9.54 ns, 11.82 ns and 18.98 ns lifetime for $FASnI_3$, PEAI- $FASnI_3$, and PEABr- $FASnI_3$, respectively, based on the curves plotted in Figure 4b. However, we find a lower decay time for partial device stacks ITO/PEDOT:PSS/PEABr-$FASnI_3$/ICBA(PCBM)/BCP, which indicates that quenching is predominantly happening by charge transport layers. When using ICBA instead of PCBM the lifetime increases from 5.4 ns to 8.42 ns, consistent with the increased PLQY.

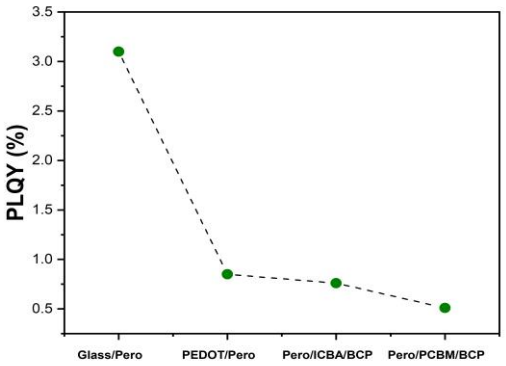

(a)

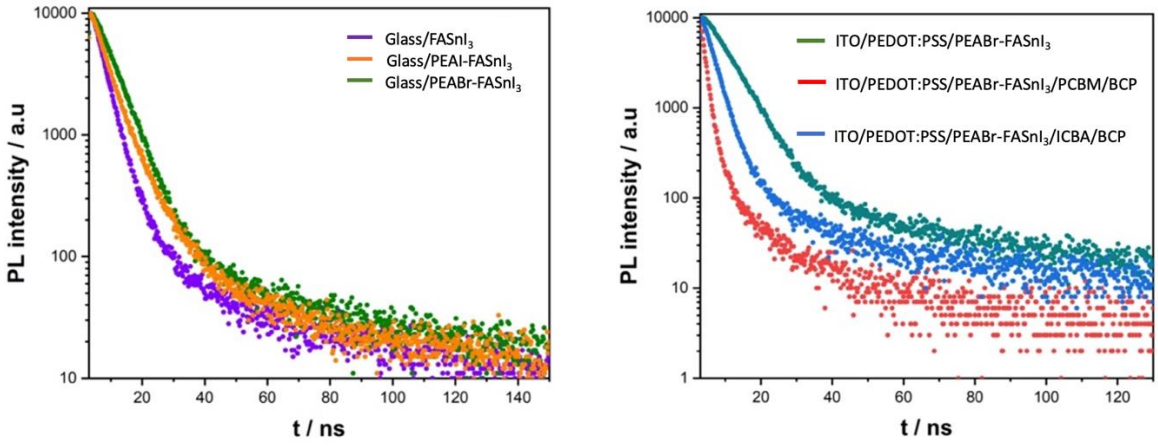

(b) (c)

Figure 4. a) PLQY of PEABr-$FASnI_3$ perovskite films with and without CTLs. Time-resolved PL (TRPL) of b) Sn-perovskite with and without additives, measured on glass and c) partial device stacks of PEABr-$FASnI_3$ with different ETLs.

Voltage analysis of Sn-based perovskite

In order to reveal the origin of the non-radiative recombination pathways at the Sn-perovskite/fullerene interface we employed Fourier-transformed photocurrent spectroscopy (FTPS). Figure 5b displays the external quantum efficiency (EQE_{PV}) spectrum of devices using PCBM and ICBA as interlayer on a logarithmic scale measured over 6-7 decades. The blueshift observed in the UV-VIS and PL spectra (Figure 3 a and b) upon adding PEABr is also visible in the FTPS spectra as a shift of the main absorption onset around 1.25 eV. A sub-gap absorption band is visible between 0.8-1.2 eV for PCBM based devices assembled with or without the PEABr additive. When substituting PCBM with ICBA, this sub-gap absorption is severely suppressed and/or blueshifted. We therefore assign the origin of this extra sub-gap absorption to the Sn-perovskite/PCBM interface, since its presence depends on the type of ETL. At this interface, charge-transfer (CT) transitions, exciting an electron from the valence band of the Sn-perovskite to the LUMO of PCBM are possible, as depicted in figure 5a. The increased LUMO of ICBA by 0.17 eV [19] as compared to PCBM is expected to result in a blue-shifted charge-transfer absorption onset. A shift of the CT absorption onset of this magnitude

would shift it beneath the main Sn-perovskite absorption, explaining the undetected sub-gap CT absorption when using ICBA as ETL.

Decay of these interfacial CT states occurs non-radiatively as electroluminescent spectra of device with PCBM as ETL do not reveal any redshift emission band consistent with CT emission (Figure 5c). Furthermore, the EQE_{EL} of the PCBM based devices at injection currents comparable to the short-circuit current under solar conditions (around 20 $mA.cm^{-2}$) is much lower than that of the ICBA based device, which is already low ($< 10^{-7}$, see below.).

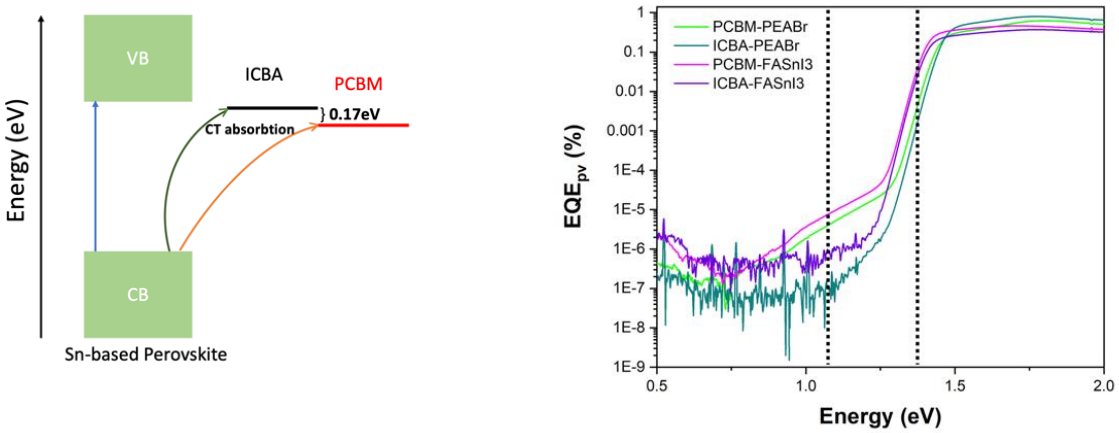

(a) (b)

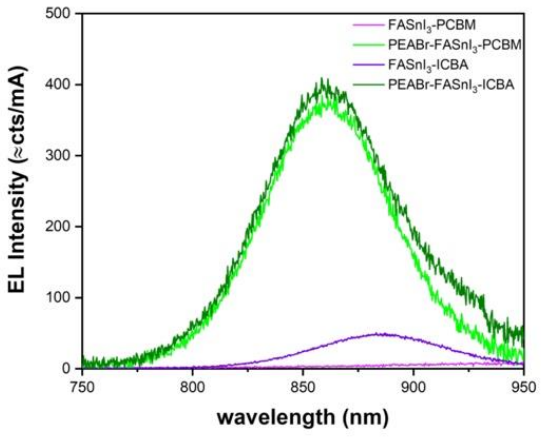

(c)

Figure 5. a) Schematic representation of charge transfer absorption at the Sn-based perovskite/fullerene interface b) Photovoltaic external quantum efficiency (EQE_{PV}) measured with Fourier transform photo-

current spectroscopy (FTPS). In the region below 1.2 eV, CT absorption is visible when PCBM is used as ETL. The dotted lines indicate the energy difference between the VB-LUMO of ICBA and PCBM. c) Electroluminescence spectra of Sn-based PSCs with and without additive and different ETLs.

The nonradiative recombination process diminishes the steady-state charge density by facilitating recombination, leading to a subsequent decrease in the open-circuit voltage (V_{OC}) of a solar cell. The EL and FTPS spectra can be used to calculate the maximum theoretical open circuit voltage of a solar cell ($V_{OC,0}$) using the following formula: [8]

$$V_{OC,0} = \frac{k_B T}{e} \ln\left(\frac{J_{SC}}{J_0} + 1\right) \quad (1)$$

Where k_B is the Boltzmann constant, T is the temperature in Kelvin, and e is the elementary charge, J_{sc} is the short circuit current density, and J_0 is the saturation current density in dark. The minimum achievable J_0 in the case of the absence of non-radiative recombination is determined by using the reciprocity relation between EQE and EL using FTPS and EL spectra.

The maximum theoretical radiative open-circuit voltage (V_{OC}^{rad}) for PEABr-$FASnI_3$ perovskite, where the bandgap (E_g) is 1.44 eV and J_{sc} equals to 20.54 mA/cm^2 at room temperature, is in this way calculated to be 1.19 V, which means that in the ideal case there would be 0.25 V of voltage deficit ($\mathbf{\Delta}V_{oc}$= (E_g/e - V_{OC}^{rad} = 0.25V). It is evident that the measured $V_{OC} = 0.68\,V$ for ICBA is significantly lower than theoretical maximum V_{OC}^{rad}. For PCBM as ETL the non-radiative voltage losses, i.e. the difference between V_{OC}^{Rad} and V_{OC} = 1.18-0.49 = 0.69 V while for ICBA it is 0.51 V (1.19 – 0.68 = 0.51 V).

An alternative way to determine these non-radiative voltage losses ($\boldsymbol{\Delta}V_{OC}^{nrad} = V_{OC}^{rad} - V_{OC}$) is by measuring the external electroluminescence quantum efficiency (EQE_{EL}) of the full device stacks operated as light-emitting diode (LED) under an injection current comparable to the

short circuit current at solar conditions. The relation between ΔV_{OC}^{nrad} and EQE_{EL} is expressed as Equation 2:[28]

$$V_{OC}^{nrad} = \frac{k_B T}{e} ln(EQE_{EL}) \quad (2)$$

When PCBM is replaced by ICBA, the device approached an EQE_{EL} value in the range of 10^{-7} at an injection current of 30 mA.cm^{-2}. Equation 2 predicts in that case a V_{OC}^{nrad} in the range of 0.41V at 298 K. This value is in the same range as the value for $V_{OC,cal}^{nrad}$ determined using the FTPS spectra (see Table 2). When using PCBM as ETL, the measured EQE_{EL} is below the detection limit of the setup. This corresponds to the much higher V_{OC}^{nrad} for PCBM devices: using equation (2), we expect an EQE_{EL} of (exp(-0.7/kT) ~ 10^{-12}), well below the detection limit of the EQE_{EL} setup. We indeed could not detect any EL for the PCBM devices, even at voltages well above V_{OC}. Table 2 summarizes the values obtained from EQE_{PV} and EQE_{EL} measurements and calculations.

Table 2. Parameters measured and calculated for quantifying non-radiative recombination losses.

perovskite	ETL	E_g (eV)	V_{OC} (V)	E_g/q-V_{OC}	$V_{OC,ca}^{rad}$ (V)	$\Delta V_{OC,cal}^{nrad}$ (V)	$EQE_{EL,cal}$	EQE_{EL} (%)	ΔV_{OC}^{nra} (V)
PEABr-$FASnI_3$	PCBM	1.44	0.49	0.95	1.18	0.69	1.77×10^{-12}	_	_
PEABr-$FASnI_3$	ICBA	1.44	0.68	0.76	1.19	0.51	2.06×10^{-9}	$<10^{-7}$	0.41

CONCLUSION

One of the primary challenges in the development of Sn-based perovskite solar cells is achieving a high open circuit voltage. By using Fourier-transform and electroluminescence spectroscopy, we have determined non-radiative voltage losses in the range of 0.41-0.51 V, which contrasts with the corresponding value for lead PSCs (with $V_{OC}^{nrad} = 0.165\ V$ [29]). A part of these non-radiative losses can be attributed to the Sn-perovskite/ETL interface: The detection of sub-gap CT absorption in the case of a PCBM ETL coincides with a large increase in non-radiative recombination in comparison to an ICBA ETL, where CT absorption is absent. This points to Sn-perovskite/fullerene CT states as sources for non-radiative recombination. This work shows that the properties and energetics of the charge-transfer states at the perovskite/fullerene interface can be manipulated to reduce the non-radiative recombination phenomenon and enhance the PCE of the Sn-based PSCs.

ACKNOWLEDGEMENT:

Funding information comes here

REFERENCES

(1) Min, H.; Lee, D. Y.; Kim, J.; Kim, G.; Lee, K. S.; Kim, J.; Paik, M. J.; Kim, Y. K.; Kim, K. S.; Kim, M. G.; et al. Perovskite solar cells with atomically coherent interlayers on SnO2 electrodes. *Nature* **2021**, *598* (7881), 444-450. DOI: 10.1038/s41586-021-03964-8.

(2) Green, M. A.; Ho-Baillie, A.; Snaith, H. J. The emergence of perovskite solar cells. *Nature Photonics* **2014**, *8* (7), 506-514. DOI: 10.1038/nphoton.2014.134.

(3) Kour, R.; Arya, S.; Verma, S.; Gupta, J.; Bandhoria, P.; Bharti, V.; Datt, R.; Gupta, V. Potential substitutes for replacement of lead in perovskite solar cells: a review. *Global Challenges* **2019**, *3* (11), 1900050.

(4) Zhang, Q.; Hao, F.; Li, J.; Zhou, Y.; Wei, Y.; Lin, H. Perovskite solar cells: must lead be replaced–and can it be done? *Science and Technology of advanced MaTerialS* **2018**, *19* (1), 425-442.

(5) Kamat, P. V.; Bisquert, J.; Buriak, J. Lead-free perovskite solar cells. *ACS Energy Letters* **2017**, *2* (4), 904-905.

(6) Abate, A. Perovskite solar cells go lead free. *Joule* **2017**, *1* (4), 659-664.

(7) Li, J.; Cao, H.-L.; Jiao, W.-B.; Wang, Q.; Wei, M.; Cantone, I.; Lü, J.; Abate, A. Biological impact of lead from halide perovskites reveals the risk of introducing a safe threshold. *Nature communications* **2020**, *11* (1), 310.

(8) Shockley, W.; Queisser, H. J. Detailed balance limit of efficiency of p-n junction solar cells. *Journal of applied physics* **1961**, *32* (3), 510-519.

(9) Yu, B. B.; Chen, Z.; Zhu, Y.; Wang, Y.; Han, B.; Chen, G.; Zhang, X.; Du, Z.; He, Z. Heterogeneous 2D/3D tin-halides perovskite solar cells with certified conversion efficiency breaking 14%. *Advanced Materials* **2021**, *33* (36), 2102055.

(10) Leijtens, T.; Prasanna, R.; Gold-Parker, A.; Toney, M. F.; McGehee, M. D. Mechanism of tin oxidation and stabilization by lead substitution in tin halide perovskites. *ACS Energy Letters* **2017**, *2* (9), 2159-2165.

(11) Hao, F.; Stoumpos, C. C.; Guo, P.; Zhou, N.; Marks, T. J.; Chang, R. P.; Kanatzidis, M. G. Solvent-mediated crystallization of CH3NH3SnI3 films for heterojunction depleted perovskite solar cells. *Journal of the American Chemical Society* **2015**, *137* (35), 11445-11452.

(12) Liao, Y.; Liu, H.; Zhou, W.; Yang, D.; Shang, Y.; Shi, Z.; Li, B.; Jiang, X.; Zhang, L.; Quan, L. N. Highly oriented low-dimensional tin halide perovskites with enhanced stability and photovoltaic performance. *Journal of the American Chemical Society* **2017**, *139* (19), 6693-6699.

(13) Shao, S.; Liu, J.; Portale, G.; Fang, H. H.; Blake, G. R.; ten Brink, G. H.; Koster, L. J. A.; Loi, M. A. Highly reproducible Sn-based hybrid perovskite solar cells with 9% efficiency. *Advanced Energy Materials* **2018**, *8* (4), 1702019.

(14) Choi, W.-G.; Park, C.-G.; Kim, Y.; Moon, T. Sn perovskite solar cells via 2D/3D bilayer formation through a sequential vapor process. *ACS Energy Letters* **2020**, *5* (11), 3461-3467.

(15) Sandhu, S.; Singh, R.; Yoo, K.; Kumar, M.; Lee, J.-J. Effect of binary additives in mixed 2D/3D Sn-based perovskite solar cells. *Journal of Power Sources* **2021**, *491*, 229574.

(16) Dong, J.; Shao, S.; Kahmann, S.; Rommens, A. J.; Hermida-Merino, D.; ten Brink, G. H.; Loi, M. A.; Portale, G. Mechanism of crystal formation in Ruddlesden–Popper Sn-based perovskites. *Advanced Functional Materials* **2020**, *30* (24), 2001294.

(17) Shao, S.; Dong, J.; Duim, H.; Gert, H.; Blake, G. R.; Portale, G.; Loi, M. A. Enhancing the crystallinity and perfecting the orientation of formamidinium tin iodide for highly efficient Sn-based perovskite solar cells. *Nano Energy* **2019**, *60*, 810-816.

(18) Cao, D. H.; Stoumpos, C. C.; Yokoyama, T.; Logsdon, J. L.; Song, T.-B.; Farha, O. K.; Wasielewski, M. R.; Hupp, J. T.; Kanatzidis, M. G. Thin films and solar cells based on semiconducting two-dimensional ruddlesden–popper (CH3 (CH2) 3NH3) 2 (CH3NH3) n− 1Sn n I3 n+ 1 perovskites. *ACS Energy Letters* **2017**, *2* (5), 982-990.

(19) Jiang, X.; Wang, F.; Wei, Q.; Li, H.; Shang, Y.; Zhou, W.; Wang, C.; Cheng, P.; Chen, Q.; Chen, L. Ultra-high open-circuit voltage of tin perovskite solar cells via an electron transporting layer design. *Nature communications* **2020**, *11* (1), 1245.

(20) Lee, M.; Kim, D.; Lee, Y. K.; Koo, H.; Lee, K. T.; Chung, I. Indene-C60 bisadduct electron-transporting material with the high LUMO level enhances open-circuit voltage and efficiency of tin-based perovskite solar cells. *ACS Applied Energy Materials* **2020**, *3* (6), 5581-5588.

(21) Liu, W.; Hu, S.; Pascual, J.; Nakano, K.; Murdey, R.; Tajima, K.; Wakamiya, A. Tin Halide Perovskite Solar Cells with Open-Circuit Voltages Approaching the Shockley–Queisser Limit. *ACS Applied Materials & Interfaces* **2023**, *15* (27), 32487-32495.

(22) Jiang, X.; Li, H.; Zhou, Q.; Wei, Q.; Wei, M.; Jiang, L.; Wang, Z.; Peng, Z.; Wang, F.; Zang, Z. One-step synthesis of SnI2·(DMSO) x adducts for high-performance tin perovskite solar cells. *Journal of the American Chemical Society* **2021**, *143* (29), 10970-10976.

(23) Jeon, N. J.; Noh, J. H.; Kim, Y. C.; Yang, W. S.; Ryu, S.; Seok, S. I. Solvent engineering for high-performance inorganic–organic hybrid perovskite solar cells. *Nature materials* **2014**, *13* (9), 897-903.

(24) Yao, H.; Zhu, W.; Hu, J.; Wu, C.; Wang, S.; Zhao, X.; Niu, X.; Ding, L.; Hao, F. Halogen engineering of 2D/3D tin halide perovskite for enhanced structural stability. *Chemical Engineering Journal* **2023**, *455*, 140862.

(25) Yang, Z.; Chueh, C.-C.; Liang, P.-W.; Crump, M.; Lin, F.; Zhu, Z.; Jen, A. K.-Y. Effects of formamidinium and bromide ion substitution in methylammonium lead triiodide toward high-performance perovskite solar cells. *Nano Energy* **2016**, *22*, 328-337.

(26) Johnston, A.; Walters, G.; Saidaminov, M. I.; Huang, Z.; Bertens, K.; Jalarvo, N.; Sargent, E. H. Bromine incorporation and suppressed cation rotation in mixed-halide perovskites. *ACS nano* **2020**, *14* (11), 15107-15118.

(27) Zhao, J.; Deng, Y.; Wei, H.; Zheng, X.; Yu, Z.; Shao, Y.; Shield, J. E.; Huang, J. Strained hybrid perovskite thin films and their impact on the intrinsic stability of perovskite solar cells. *Science advances* **2017**, *3* (11), eaao5616.

(28) Tress, W.; Marinova, N.; Inganäs, O.; Nazeeruddin, M. K.; Zakeeruddin, S. M.; Graetzel, M. Predicting the open-circuit voltage of CH3NH3PbI3 perovskite solar cells using electroluminescence and photovoltaic quantum efficiency spectra: the role of radiative and non-radiative recombination. *Advanced Energy Materials* **2015**, *5* (3), 1400812.

(29) Ren, A.; Lai, H.; Hao, X.; Tang, Z.; Xu, H.; Jeco, B. M. F. Y.; Watanabe, K.; Wu, L.; Zhang, J.; Sugiyama, M. Efficient perovskite solar modules with minimized nonradiative recombination and local carrier transport losses. *Joule* **2020**, *4* (6), 1263-1277.